Tropical Aquatic and Soil Pollution

*Research Article*
**Volume 4(2), 2024, 127–142**
https://doi.org/10.53623/tasp.v4i2.497

# Synthesis of Aluminum Oxide Nanoparticle Adsorbents from Waste Aluminum Foil and Assesses Their Efficiency in Removing Lead (II) Ions from Water

**Md. Aktaruzzaman[1], Sayed M.A. Salam[2], M.G. Mostafa[1]***

[1]Water Research Lab, Institute of Environmental Science, University of Rajshahi, Rajshahi 6205, Bangladesh
[2]Department of Applied Chemistry and Chemical Engineering, University of Rajshahi, Rajshahi 6205, Bangladesh

*Correspondence: mostafa_ies@yahoo.com

**SUBMITTED: 16 September 2024; REVISED: 21 October 2024; ACCEPTED: 24 October 2024**

**ABSTRACT:** Aluminum oxide nanoparticles have recently been applied to water treatment as adsorbents by researchers. In this study, aluminum oxide nanoparticles (AlONPs) were synthesized using scrap aluminum foil through a straightforward, inexpensive, and green approach, and their performance in adsorbing lead (II) ions from an aqueous solution was assessed. The synthesized nanoparticles were characterized using Fourier Transform Infrared Spectroscopy (FTIR), X-ray Diffraction (XRD), Transmission Electron Microscopy (TEM), and Scanning Electron Microscopy with Energy-Dispersive X-ray Spectroscopy (SEM-EDX) to analyze their bonding nature, particle size, phase composition, and surface morphology. They exhibited an average particle size of 32.73 nm, consisting predominantly of γ-$Al_2O_3$, with small amounts of α-$Al_2O_3$ and a minor unknown phase. The lead adsorption efficiency was evaluated under optimized parameters, including pH, contact time, and doses of both adsorbate and adsorbent. The results demonstrated that the AlONPs achieved a 98% removal efficiency within 30 minutes of contact time at a pH of 5.5. Additionally, the Freundlich adsorption isotherm model ($R^2$ value of 0.9972) and the pseudo-second-order kinetic model ($q_e$) value of 37.97 mg/g) were shown to fit the lead adsorption process better than other models. Hence, the synthesized AlONPs offer potential as nanoparticle adsorbents for removing lead (II) ions from aqueous solutions.

**KEYWORDS:** Aluminum foil; characterization; nanoparticles; adsorption isotherm; adsorption kinetics

## 1. Introduction

A major proportion of aluminum foil was used for the packaging of food, cosmetics, chemical products, and thermal insulation. The used aluminum foils were discarded in the environment, producing long-lasting waste that had negative impacts on the environment and ecosystem. Many strategies had been used to lessen the amount of aluminum debris that ended up in the

environment. Recycling of waste aluminum was the most common approach [1]. Nevertheless, recycling had several drawbacks and ultimately led to increased pollution. This was because it involved shredding, melting, and compressing the aluminum trash into something new that required strong machinery. The majority of these operations relied on burning fossil fuels like coal, a major source of sulfur and nitrogen oxide emissions that polluted the air [2]. Furthermore, melted aluminum led to several health issues, such as immune system deterioration, inflammation of the skin, liver damage, and certain types of cancer [3]. Greener recycling techniques were therefore necessary. Making aluminum oxide nanoparticles from discarded aluminum foil and using them as adsorbents to treat contaminated water was a preferable option.

As in many other developing nations, in Bangladesh, groundwater was the main source of potable water. Due to its superior microbiological and chemical quality and low treatment requirements, it was regarded as a safer source of drinking and cooking water. The majority of the water supply in rural areas of Bangladesh came from hand-pump tube wells [4]. Groundwater was also a major source of water for metropolitan areas [5]. But recently, groundwater contamination by heavy metals due to both anthropogenic and geogenic reasons had become a matter of concern [6]. The permissible standard lead concentration levels in drinking water set by BDWS (2019), WHO (2011), and USEPA (2019) were 0.05, 0.01, and 0.015 mg/L, respectively, and the lead concentration of 37.50% of total pumps in Bangladesh that drew groundwater exceeded all the standard guideline limits [7]. Another study found that the acceptable level of Pb, Fe, and Mn in Rajshahi's drinking water was significantly greater than that recommended by the WHO [8]. A trace quantity of lead became more toxic to humans than other heavy metal contaminants [9]. For humans, Pb consumption beyond the allowable level could trigger cancer. Children were more susceptible than adults to both the short- and long-term consequences of lead exposure. Adults subjected to lead experienced long-term adverse consequences, such as an elevated risk of hypertension. Exposure to excessive amounts of lead resulted in anemia, weakness, and harm to the kidney, DNA, brain, and the developing baby's nervous system [10]. A recent study showed that groundwater in northern Bangladesh contained heavy metals. As, Fe, Mn, and Pb in the groundwater of Rajshahi city, Bangladesh, were well beyond the drinking water standard of the WHO [11]. Heavy metals released into the environment posed significant risks to the ecosystem and human health because of their toxicity and long half-lives [12].

Therefore, it was imperative to find efficient techniques for removing heavy metals from drinking water. The adsorption technique was a widespread, practical, economical, and efficient method with significant potential for the removal, recycling, and recovery of potentially hazardous metals from water [13-15]. Metal oxide nanoparticles were the most widely used adsorbents due to their low cost, ease of fabrication, large surface area, high mechanical properties, resistance to thermal degradation, ease of modification, high adsorption capacity, and variety of surface functionalization options that enhanced selectivity in the elimination of metal ions from the solution. Alumina nanoparticles were one of the significant types of metal oxides and had enormous technological, industrial, and environmental engineering applications [16-17].

A recent study reported on the preparation of aluminum oxide nanoparticles from scrap aluminum foil and their use in aluminum ion cells [18] and the removal of methylene blue dye

from water [19]. No study so far had investigated lead removal using nanoparticles derived from aluminum foil waste. In this study, aluminum foil debris that had accumulated and become environmentally harmful was collected and transformed into aluminum oxide nanoparticles (AlONPs), and their efficiency in removing lead (II) ions from water was assessed. The research focused on synthesizing aluminum oxide nanoparticles (AlONPs) from aluminum foil waste through an eco-friendly and green approach and investigating their potential application as adsorbents to remove lead (II) ions from water. Thus, it was a green process, as it reduced pollution while using waste foil and producing valuable adsorbents for water purification. The characterization of aluminum oxide nanoparticles (AlONPs) and their performance in removing lead (II) ions from water, as well as adsorption isotherms and kinetic modeling, were conducted in this study.

## 2. Materials and Methods

2. *Synthesis of Aluminum Oxide Nanoparticles (AlONPs).*

Waste aluminum foils were collected from various waste bins on the campus of the University of Rajshahi. Afterward, 20 g of cleaned, dried, and cut foil pieces were added to a mixture of 110 ml of hydrochloric acid (36% v/v) and 110 ml of water, continuing until the chemical reaction was completed and the effervescence stopped [18]. Once cooled, the solution was filtered using Whatman No. 42 (W42) filter paper to remove impurities. A 1M $Na_2CO_3$ solution was then added from a burette at a rate of one drop per second, with continuous agitation (100 rpm) using a magnetic stirrer, until a gelatinous precipitate of aluminum oxide was formed. To eliminate NaCl and other impurities from the precipitate, distilled water was added, allowing the solution to settle for an hour. The transparent liquid was decanted, more water was added, and the process was repeated three times to fully remove the NaCl. After filtering, aluminum oxide gel was obtained, which was dried for 48 hours at 70°C and transformed into powder. The powder was then calcinated at 550°C for three hours and subsequently ground into alumina nanoparticles using a mortar and pestle.

3. *Characterization of the nanoparticles.*

A Carbolite RHF-1500 muffle furnace was used for calcination, and the crystallite phase, structure, and average size of the nanoparticles were determined by X-ray diffraction (XRD) using a Rigaku smart lab X-ray diffractometer. Fourier Transform Infrared (FTIR) spectroscopy (Perkin Elmer, Spectrum 100) was employed to confirm the bonding nature of the nanoparticles. The microstructure, homogeneity, particle size, and detailed crystallographic and morphological features were examined using a Thermo Scientific Talos F200X Transmission Electron Microscope (TEM). Surface topography, crystallographic data, and composition were analyzed using a Joel field emission scanning electron microscope (FESEM-EDS, model JSM IT800). Finally, lead (II) ion concentration in the solution phase was measured using a Shimadzu atomic absorption spectrophotometer (AA-6800).

4. *Batch adsorption process.*

Equations (1) and (2) were used to calculate the percentage of metal ions removed by the adsorbents and the equilibrium adsorption capacity of the adsorbents.

$$\%R = \frac{(C_o - C_e)}{C_o} \times 100\% \quad (1)$$

$$q_e = \frac{(C_0 - C_e)}{W} \times V \quad (2)$$

In this case, $V$ represents the lead II ion-containing solution's volume in L, $w$ denotes the adsorbent's weight in g, $C_0$ and $C_e$ indicate the lead II ion's initial and equilibrium concentrations in mg/L, respectively, and $q_e$ denotes the adsorbent's equilibrium adsorption capacity in mg/g of adsorbent.

5. *Assessment of adsorption efficiency.*

Lead (II) nitrate [$Pb(NO_3)_2$] salt was used as a source of lead (II) ions in the adsorption experiment. A stock solution of 1000 ppm of $Pb^{2+}$ ions was prepared by dissolving the salt in deionized water. From this stock solution, experimental solutions with the appropriate concentrations were prepared. Adsorption equilibrium was examined across a pH range of 3–8 to determine the ideal pH for maximum lead removal at room temperature. To assess the effect of contact time, 0.25 g of AlONPs adsorbent was mixed with 250 mL of Pb(II) ion solution at a concentration of 25 ppm, with the pH adjusted to 5.5. The solution was shaken, and 25 mL of the sample was collected at different intervals (10, 20, 30, 40, 50, 60, 90, 120, 160, and 190 minutes). The concentration of lead in the solution was determined using Atomic Absorption Spectroscopy (AAS). To evaluate the effect of adsorbate dose, solutions of $Pb(NO_3)_2$ were prepared with concentrations of 1, 2, 3, 4, 5, 10, 20, 30, 40, and 50 ppm. Each solution (25 mL) was transferred to a conical flask, adjusted to a pH of 5.5, and 0.025 g of AlONPs was added. After shaking for 50 minutes at 60 rpm at room temperature (32 °C), the suspensions were separated, and the remaining lead concentration was measured. For studying the effect of AlONP dose on Pb(II) ion adsorption, 25 ppm $Pb(NO_3)_2$ solutions were prepared. To six conical flasks, 0.01, 0.02, 0.03, 0.04, 0.05, and 0.06 g of AlONPs were added, and the pH was adjusted to 5.5. After shaking for 30 minutes at room temperature, the suspensions were separated, and the remaining lead concentrations were analyzed to assess adsorption efficiency..

6. *Adsorption isotherm study.*

The Langmuir equation, commonly applied for monolayer sorption on a surface with a finite number of identical sites, is as follows :

$$\frac{1}{q_e} = \frac{1}{q_m} + \frac{1}{bq_m C_e} \quad (3)$$

Where $q_m$ is the highest monolayer coverage-corresponding adsorption capacity (mg/g) and the Langmuir constant $b$ is a quantitative indicator of the binding sites' affinity that corresponds to the energy of adsorption (l/mg), the quantity of solute on the surface of the adsorbent is denoted by $q_e$ (mg/g), Ce is the concentration of ions in the solution at equilibrium (mg/l), and a straight line is shown when $1/q_e$ and $1/c_e$ are plotted. From the plots' intersection and slope, respectively, one can determine the values of $q_m$ and b.

An empirical equation, known as the Freundlich model can be used to illustrate heterogeneous adsorption systems represented as:

$$logq_e = log\ K_F + 1/n\ log\ C_e \quad (4)$$

The equilibrium solute concentration on the adsorbent ((mg/g) and the equilibrium solute concentration in solution (mg/l) are represented by the variables $q_e$ and $C_e$, respectively. The constants of the Freundlich equation, $K_F$ (mg/g) and n reflect the adsorption intensity and capacity, respectively [20]. Based on this model, whenever the $logq_e$ vs. $logC_e$ plot is drawn, the straight line's intercept and slope provide the $K_F$ and n values, repectively. Additionally, this equation was applied to evaluate experimental data pertaining to the impact of initial concentrations of heavy metal adsorption on the adsorbent.

7. *Adsorption kinetics.*

Using the pseudo first order and pseudo second order formulas, the adsorption kinetics of lead (II) ions onto AlONP surfaces are demonstrated. A simple method to illustrate the pseudo first order linear form is as:

$$ln(q_e - q_t) = lnq_e - K_1 t \quad (5)$$

where, $K_1$ (/min) denotes the pseudo-first-order adsorption rate constant, the amount of metal ion sorbed at the state of equilibrium is expressed as $q_e$ (mg/gof dry weight), and the amount of metal ion on the sorbent surface at any given time t (minutes) is expressed as $q_t$ (mg/g of dry weight). A common way to express the pseudo-second-order equation is as :

$$\frac{t}{q_t} = \frac{1}{K_2\, q_e^2} + \frac{t}{q_e} \quad (6)$$

Where, $K_2$ (g/mg.min) is the pseudo-second order adsorption rate constant.

*2.7. Desorption experiments.*

After the adsorption of Pb (II) ions from water, the AlONPs were separated by centrifugation and washed with deionized water to remove any unabsorbed and loosely bonded lead ions. The process was repeated by adding deionized water, centrifuging the solution for 10 minutes at 3000 rpm, and then drying the AlONPs for two hours at 60°C in an oven. The lead ion-adsorbed AlONPs were subsequently mixed with 50 mL of a 1 M HCl solution, shaken for two hours, and centrifuged at 2000 rpm for five minutes. The resulting supernatant was sent for analysis using AAS to determine the concentration of desorbed lead ions. The AlONPs were then cleaned with deionized water, dried at 100°C for two hours, and reused for additional Pb (II) ion adsorption. This adsorption-desorption cycle was repeated three times to assess the recyclability of the AlONPs. The following equation was employed to calculate the Pb (II) ion recovery efficiency [21].

$$Recovery(\%) = \frac{(amount\ of\ desorbed\ lead\ ions)}{(amount\ of\ adsorbed\ lead\ ions)} \times 100 \quad (7)$$

## 3. Results and Discussion

*3.1.Characterization of the synthesized nanoparticles.*

### *3.1.1. XRD Analysis.*

The sharp peaks of the XRD diffractograms (Figure 1) indicate that the sample has crystallite structure. The observed data was properly matched with the value of standard JCPDS/ICDD crystal system data (Card No. 00-010-0425), and the prominent peaks of the x-ray diffractograms were matched as follows: 2θ angle: 25.34 (012), 27.50 (111), 31.83 (200), 45.55 (220), 56.56 (222), 57.53 (116), 67.03 (400), 75.37 (420). The most prominent peak was found at angle 2θ = 31.83 (200) with 267 cps, which indicates the presence of α- $Al_2O_3$, which has boehmite crystal structures [22]. Peaks at 36.83°(331) with 23 cps, 45.55°(220) with 179 cps, 56.56°(222) with 100 cps, and 67.03°(400) with 40 cps correspond to γ-$Al_2O_3$ [18]. So, it is interesting that both the α and γ phases coexist within the synthesized nanoparticles. This remarkable finding deserves additional investigation. Besides these two polymorphs, the synthesized nanoparticles had some unknown phases also. Probably this happened because in the quantification process, using a reference alpha, beta, or gamma standard could produce extremely unpredictable results [23]. The average particle size was calculated by using the Scherrer equation (equation 8) based on X-ray diffraction data, and it was found that the average crystallite size is 32.73 nm .

$$D = \frac{K\lambda}{\beta.cos\theta}\ (nm) \tag{8}$$

Where, $D$=Crystallite size (nm), $\beta$= Line Broadening at FWHM (Radians), $\theta$(Bragg Angle) = Peak Position (Radians), $\lambda$= Wavelength of X-ray = 0.15418 nm, $K$= Related to Scherrer constant = 0.94

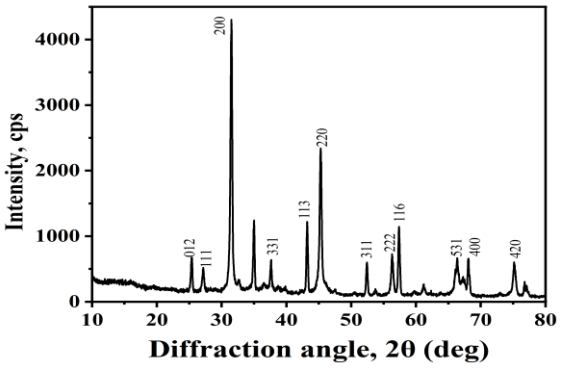


**Figure 1.** XRD Pattern of the synthesized AlONPs from waste aluminum foil.

### *3.1.2. FTIR analysis.*

FTIR spectra are displayed in Figure 2. Before lead adsorption [Figure 2(a)] by the AlONPs, the prominent peaks at 3435 $cm^{-1}$ and 1638 $cm^{-1}$ are due to bending and stretching of O-H functional group [24] from Al-OH framework. Peaks at 3435 $cm^{-1}$ also indicated the presence of moisture in the sample. This may happen during the experiment, as aluminum oxide nanoparticles have moisture absorption properties [25]. The band at 1385 $cm^{-1}$ refers to the typical bending vibration of $Al_2O_3$ nanoparticles lattice structure. Peaks at 595 $cm^{-1}$and 823$cm^{-1}$ support the stretching vibrations of the Al-O bond noticed in the $AlO_4$ and $AlO_6$ frameworks in the ranges of 500-700 and 700-900$cm^{-1}$, respectively. Peaks between 500-700$cm^{-1}$ and 700-900$cm^{-1}$ indicates the presence of γ-phase [26]. The absorption peak at 457$cm^{-1}$ is due to the Al–O vibration of α-$Al_2O_3$ [27]. After the adsorption of lead by the AlONPs, shifting of peaks

position, changing intensities, disappearance and generation of some new peaks of FTIR spectra [Figure 2(b)] suggest the involvement of lead atoms on the surface of the nanoparticles. The peaks at 3435 $cm^{-1}$, 1638 $cm^{-1}$ and 823 $cm^{-1}$ of Figure 2(a) shifted to 3459 $cm^{-1}$, 1635 $cm^{-1}$ and 828 $cm^{-1}$ after the adsorption of lead atom and the intensity of peaks at 1635 $cm^{-1}$ decreased [Figure 2(b)]. New peaks at 1096 $cm^{-1}$, 637 $cm^{-1}$, 505$cm^{-1}$, 448 $cm^{-1}$, and 384 $cm^{-1}$ are probably due to the vibration of Pb-O bonds [28] which creates after lead adsorption.

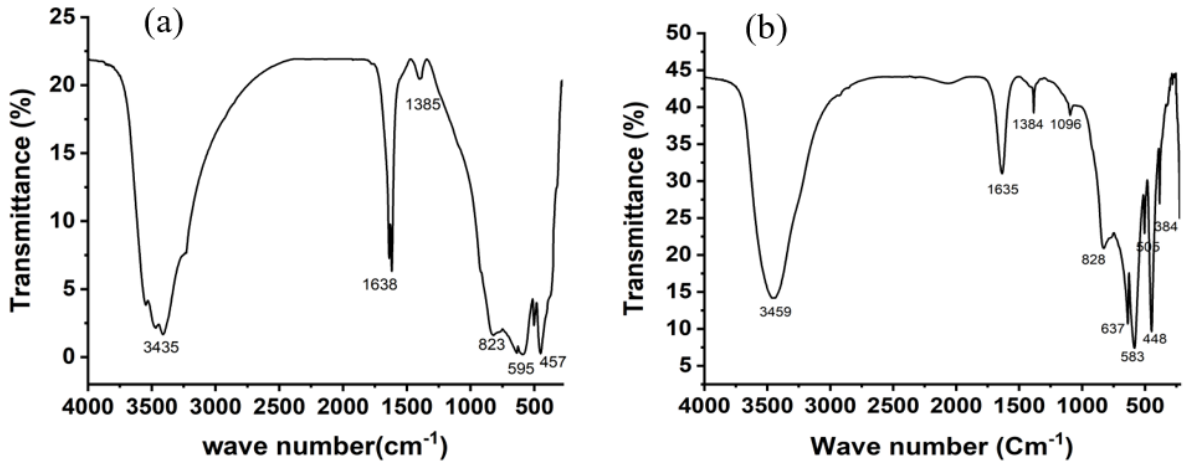


**Figure 2.** FTIR spectra of the AlONPs (a) before Pb (II) ion adsorption (b) after Pb (II) ion adsorption.

### *3.1.3. TEM analysis.*

The size, shape, crystallographic structure, and chemical composition of a variety of nanomaterials can be analyzed using transmission electron microscopy (TEM) [29]. From the photograph (Figure 3), it is clear that the nanoparticles had polymodal crystallinity and had a mixture of irregular spherical, cubic, hexagonal, and tetragonal crystals. Most of the crystal was a single particle with slight overlap, and there was a tendency of agglomeration of the nanoparticles, and this might have happened due to the result of the Vander Waal bonds that form between the particles [29, 30]. It is also clear that the surface of the synthesized nanoparticles was porous and had an average particle diameter within the nanometer range.

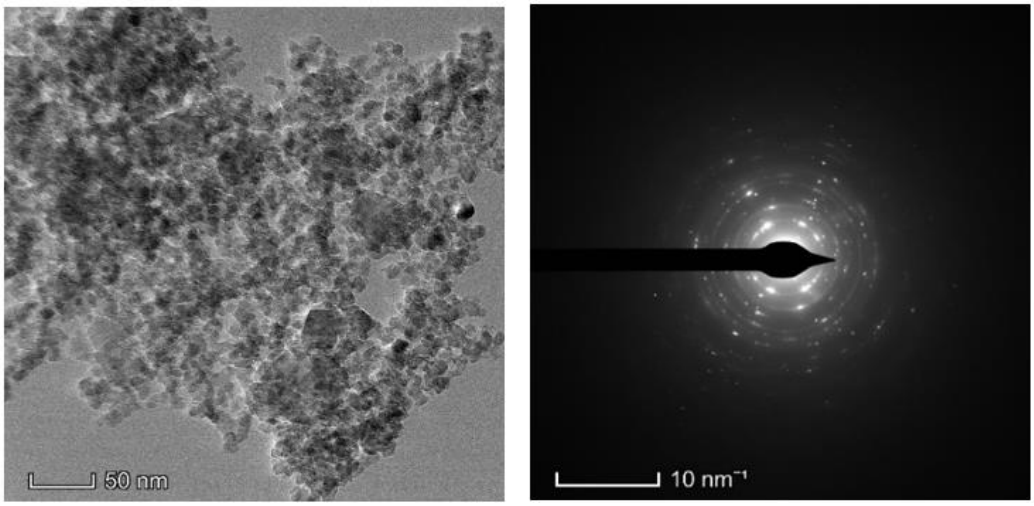


**Figure 3.** TEM images of the synthesized AlONPs.

### *3.1.4. SEM-EDX analysis.*

The SEM micrographs of the nanoparticles are shown in Figures 4 (a) and 4 (b) to know about their surface texture and morphology. From the micrographs, it is found that the samples have a rough surface with many porosities before lead adsorption (Figure 4a). These significant numbers of heterogeneous pores might be helpful for heavy metal adsorption. Careful observation reveals that the number of pores and surface roughness decreased after lead adsorption (Figure 4b). The SEM images also clarify that the nanoparticles are in the nanoscale range, and the shape of the particles is highly heterogeneous and not uniform, and a similar observation was reported [31]. Various orientations of the edges of the crystal correspond to multiple planes. The EDX (Energy Dispersive X-ray Spectroscopy) image confirmed the 100 percent elemental purity of nanoparticles because of the presence of 47% of Al and 53% of O atoms before lead adsorption, which is depicted in Figure 4(c). After the adsorption study, the spectra of lead, oxygen, and aluminum (50.06 % of Al, 41.64% of O, and 8.30% of Pb) were found (Figure 4d). This finding clearly proved that adsorption of lead (II) ions happened on the surface of nanoparticles. Since real water contains a tiny amount of lead, a very low-level adsorbate concentration was used in this case, and after lead adsorption, this sample was used for EDX analysis. So, the surface of the adsorbent is not fully saturated. Probably this is the reason for a getting significant proportion of Al and O and only 8.30% of Pb after adsorption.

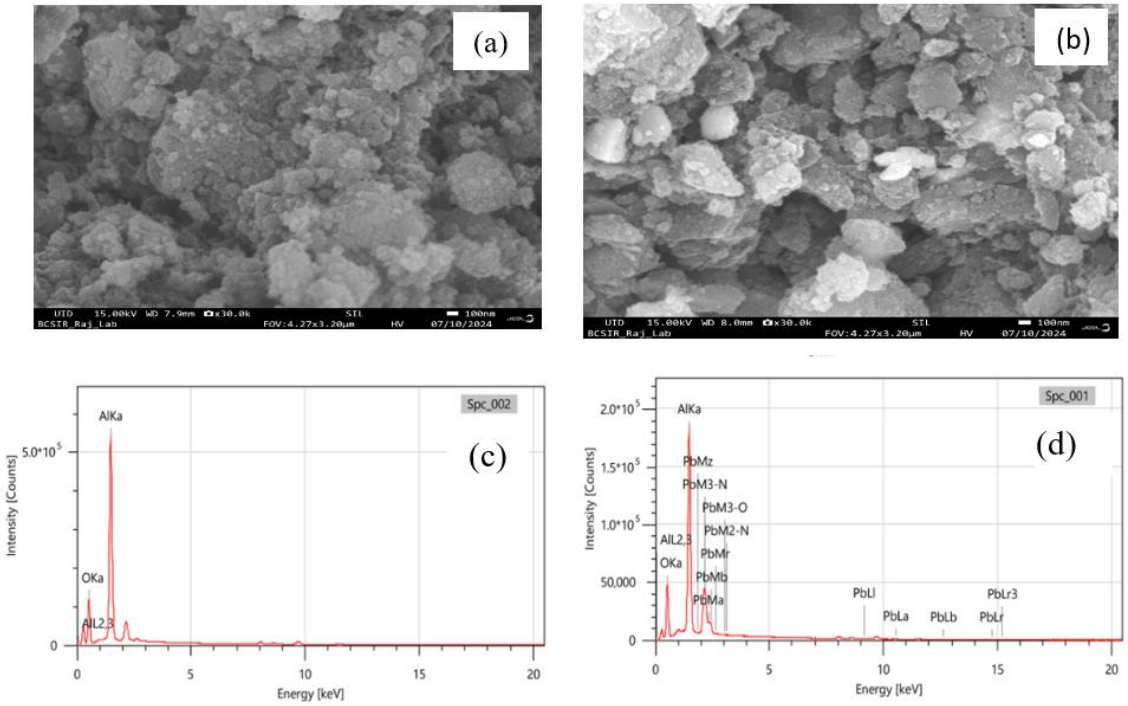


**Figure 4.** SEM images of the Synthesized AlONPs (a) before Pb adsorption, (b) after Pb adsorption (c) EDX image before Pb adsorption, (d) after Pb adsorption.

### *3.1.5. Point zero charge.*

The synthesized AlONPs' point zero charge was found to be very close to 5, which indicates that the adsorbent becomes electrically neutral and has no net surface charge at pH 5. So, the sorbent's surface is not favorable to lead adsorption below this pH because it is electrically positively charged below that level and negatively charged above pH 5, which promotes lead ion adsorption. The pH drift method was employed to determine point zero charge [30].

### *3.2.Adsorption efficiency assessment.*

### *3.2.1. Effect of pH.*

An essential factor in the adsorption of metal ions from aqueous solutions is the pH of the solution, which influences the surface charge of the adsorbent. There is an optimal pH for the adsorption process due to the competition between proton and metallic cations in a strongly acidic environment [32]. The surface becomes positively charged when the active sites are protonated, which reduces the probability of successive metal ion adsorption in solution on the surface [16]. At higher pH levels, metallic cations precipitate as a result of hydroxyl anions' interfering effects [33]. The equilibrium adsorption was examined throughout a pH range of 3–8 in order to identify the ideal pH for the highest level of lead removal. With an increase in pH, lead (II) ion removal efficiency increased because the competition between hydrogen ions and metal ions decreased. Additionally, the removal efficiency declined after an optimal pH of 5.5 (Figure 5A). For pH values of 3, 4, 5, 6, 7, and 8, the lead removal efficiency were 73%, 92%, 95%, 98%, 90%, and 82% correspondingly.

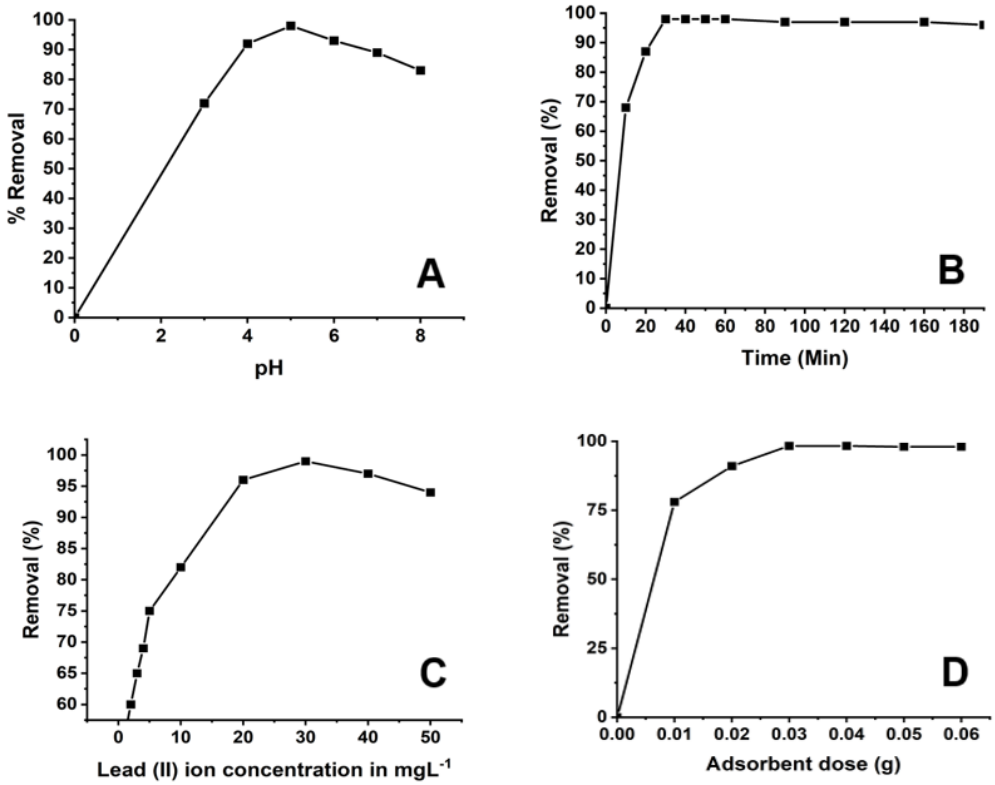


**Figure 5.** pH affects lead removal efficiency (A); Lead removal efficiency as a function of contact time (B); Effect of adsorbate dose (initial lead ion concentration) on removal efficiency (C); Adsorbent dose's impact on removal efficiency (D); contact time 30 minutes, lead concentration 25 mg/dm$^3$, pH 5.5.

### *3.2.2. Effect of contact time.*

The impact of contact time on the percentage of lead (II) ions removed by AlONPs was also studied. In Figure 5(B), the percentage of metal ions removed is plotted against contact time. After 30 minutes, the lead (II) ion removal efficiency achieved its maximum value, and for contact times up to 120 minutes, there was no noticeable improvement. This could be as a result of the high initial solute concentration and maximum initial unoccupied position of all adsorbent sites. As time went on, the adsorbent sites were filled, and the Pb(II) ion concentration gradient decreased [34]. Because of this phenomenon, a drop in adsorption rate

after a certain time resulted and became constant when equilibrium was reached [35]. Another cause of this decrease in adsorption rate is that after a certain time, the adsorbed metal ions covered the vacant spaces, creating a repulsive force among them in the adsorbent surface and in bulk phase, which lowers the adsorption rate [36]. Therefore, it was decided that 30 minutes was the ideal contact time for the lead (II) ion to adsorb by AlONPs.

### *3.2.3. Effect of adsorbate dose.*

The initial concentration of Pb (II) ions affects the removal efficiency of Pb (II) ions on the surface of AlONPs. Figure 5(C) demonstrates that when the initial concentration was raised from 1 ppm to 30 ppm, the removal percentage of Pb (II) ions increased by approximately 44%. With a higher metal concentration, this phenomenon might be caused by an excess of the concentration gradient's driving power, which may overcome the strength of mass transfer between the solid and liquid phases[37]. When the adsorbate concentration exceeds 30 ppm, the removal percentage gradually decreases. This is the consequence of the increase in the number of lead molecules that are available per adsorption site [38]. As a result, the percentage of adsorption falls for a given amount of adsorbent.

### *3.2.4. Effect of adsorbent dose.*

The number of binding sites and the total specific surface area of the adsorbent depend on the adsorbent dosage, which has a significant role in the process of adsorption [39]. Figure 5(D), displayed that with 0.03 g of the adsorbent dosage, the adsorption reached its highest point, and the maximum percentage removal of Pb (II) ions was around 98% by the synthesized AlONPs. These results are explained by the adsorbent's surface area, which increases with higher doses and creates more active sites for the removal of lead ions from the solution. Findings reported in the literature [40] are consistent with this explanation. However, when the adsorbent dose exceeded 0.03 g, the percentage removal of lead remained almost the same. This less adsorption may have happened as a result of the small adsorbate in the medium being exposed to a significant number of accessible binding sites. Cell aggregation and a subsequent reduction in intercellular distance may be caused by the massive adsorbent amounts. In addition, it formed a "screen effect" in a thick layer of cells, which "protected" binding sites from metal ions [41].

### *3.2.5. Adsorption isotherm.*

By fitting the equilibrium adsorption data on the Langmuir and Freundlich isotherms model, the sorption behavior of Pb (II) ions on AlONPs was examined. From Table 1, it is clear that the coefficient of determination ($R^2$) value was higher in the case of the Freundlich adsorption isotherm than the Langmuir adsorption isotherm model, which supports multilayer coverage of Pb (II) onto the surface of AlONPs, and adsorption happened at heterogeneous sites within the nanoadsorbent. Freundlich isotherm constant ($n$), an empirical parameter, changes with the degree of heterogeneity and should have a value between 1 and 10 (i.e. $1/n < 1$) for optimum adsorption [42]. The intensity of adsorption is reflected in the values of $n$. The values of $n$ determined from the adsorption experiment represented a favorable adsorption. For Pb(II) ion adsorption, the magnitude of $1/n$ with its value of 0.622 ($0.1 < 1/n < 1$) indicated that the adsorption of Pb(II) on AlONPs was favorable [43].

**Table 1.** Adsorption of Pb (II) ion on AlONPs adsorbent: Langmuir and Freundlich isotherm parameters.

| Langmuir model | | | Freundlich model | | |
|---|---|---|---|---|---|
| $q_m$ (mg/g) | $K_L$(min$^{-1}$) | $R^2$ | $K_F$ (mg/g) | $n$ | $R^2$ |
| 35.48 | 0.5849 | 0.8231 | 9.9744 | 1.607717 | 0.9972 |

### *3.2.6. Adsorption kinetics.*

After fitting the adsorption kinetic data to Eqaution (5) and (6), the computed outcomes displayed in Table 2. The correlation coefficients ($R^2$) of the pseudo-second-order adsorption model were found to be higher than the pseudo-first-order adsorption models and the obtained result matches with the findings of Wang and his cowokers [44]. The different research parameters for kinetics are shown in Table 2, where it is observed that there is a good agreement between the theoretical pseudo-second order kinetics ($q_e$, mg/g) model and the experimental value of adsorption capacity ($q_e$, mg/g). Consequently, the adsorption data were satisfactorily explained by the pseudo-second-order kinetic model.

**Table 2.** Kinetic parameters of Pb (II) ion adsorption on AlONPs adsorbent.

| Pseudo 1st order reaction | | | Pseudo 2nd order reaction | | |
|---|---|---|---|---|---|
| $q_e$ in mg/g | $K_1$ in min$^{-1}$ | $R^2$ | $q_e$ in mg/g | $K_2$ in g/mg.min | $R^2$ |
| 27.27 | 0.01691 | 0.7636 | 37.97 | 0.00641 | 0.99366 |

### *3.2.7. Adsorption mechanism.*

Even when the pH is far below the point zero charge, there is noticeable adsorption of Pb(II) onto hydrous $Al_2O_3$ from diluted solutions [45]. Pb(II) species hydrolyze when pH increases, with a known equilibrium constant [46].

$$Pb(II) + OH^- \longrightarrow Pb(OH)^+, \qquad Pb(OH)^+ + OH^- \longrightarrow Pb(OH)_2$$

Surfaces form a double layer when they naturally charged. When $H^+/OH^-$ ions are the surface charge determining ions, the pH of the liquid in which the solid is immerged, affects the net surface charge. The concentration of $H^+$ ions decreases as the pH of the solution rises, pushing the reaction to the right hand side. The following equation illustrates how bivalent metal ions adsorption takes place onto alumina adsorbent [34].

$$AlOH + Pb^{2+} \longrightarrow AlOPb^+ + 2H^+$$

Adsorbed ions that remain their hydration sphere during adsorption are known as "outer sphere" complexes, while ions that lose all or a portion of their hydration spheres and become directly attached to the oxide are known as "inner sphere" complexes. Adsorption of Pb(II) occurs in the presence of a positively charged alumina surface. This adsorption behavior is consistent with the formation of inner sphere complexes [45] as bellow.


Since agglomeration of nanoparticlesn can significantly lowers the interfacial spaces and surface area which can ultimately reduces its adsorption capacity, using it as soon as possible after synthesis or storing it in airtight vials gives better result.

### *3.2.8. Desorption studies.*

Regenerating the adsorbent for further applications is essential for reducing the cost of the adsorption process. The effectiveness of the recycled AlONPs in removing Pb (II) ions from water is displayed in Table 3. It was noticed that the Pb (II) ion adsorption efficiency of the recycled adsorbent was 95% even after 1st times of recycling and the efficiency significantly decreased during the 2nd and 3rd times of recycling. This happened because during the shaking process, agglomeration and gelatinous hydroxide forming tendency of the synthesized AlONPs were observed.

**Table 3.** Pb (II) ion removal efficiency by regenerated AlONPs.

| Number of repetitions | Stripping solution | Pb (II) ion removal efficiency |
|---|---|---|
| 1 | 1M HCl | 95% |
| 2 | 1M HCl | 80% |
| 3 | 1M HCl | 55% |

## 4. Conclusions

Due to their large surface area and adjustable surface morphology, aluminum oxide nanoparticles are highly versatile adsorbents. In this study, aluminum oxide nanoparticles were synthesized by dissolving aluminum foil debris in an HCl solution and gradually adding a $Na_2CO_3$ solution. FTIR, XRD, TEM, and SEM-EDX analyses indicated that the synthesized nanoparticles are polycrystalline, containing both α and γ phases, along with a minor amount of an unknown phase, and have an average diameter of 32.73 nm. This study evaluated the effectiveness of the synthesized $Al_2O_3$ nanoparticles as adsorbents for removing lead (II) ions from aqueous solutions. The results showed that the removal efficiency of lead (II) ions increased with higher initial concentrations and longer contact times, reaching optimal results at 30 minutes. Additionally, the maximum lead removal efficiency occurred at a pH of 5.5; however, when the pH exceeded 6 or fell below 3, the removal percentage decreased significantly. Furthermore, the findings revealed that the adsorption of Pb (II) ions by the nanoparticles adhered to the multilayer adsorption isotherm model ($R^2 = 0.9972$) and followed the pseudo-second-order kinetic model ($q_e$ value = 37.97 mg/g). Therefore, the synthesized nanoparticles have potential as effective and low-cost adsorbents for removing lead (II) ions from aqueous solutions. However, their regeneration efficiency significantly decreased after the second use, and they exhibited a tendency to agglomerate in aqueous solutions.

## Acknowledgments

I would like to sincerely thank all of my fellow colleagues of the Water Research Lab, Institute of Environment Science, University of Rajshahi, for their insightful criticism and fantastic teamwork, which enriched me throughout the research. I am also grateful to the Institute of Environment Science, University of Rajshahi, for providing lab facilites.

## Author Contribution

Without the constant assistance and direction of professor Md. Golam Mostafa, Institute of Environmental Science, University of Rajshahi, this research paper could not have been completed. So, I would like to give him a special thanks. I would also like to express my gratitude to professor Sayed M A Salam, Department of Applied Chemistry and Chemical Engineering, University of Rajshahi, for his valuable feedback and constructive suggestion throughout the M.Phil. programme.

## Competing Interest

The authors declare no conflicts of interest.

## References

[1] Yusuf, N.K.; Lajis, M.A.; Ahmad, A. (2019). Multiresponse optimization and environmental analysis in direct recycling hot press forging of aluminum AA6061. *Materials*, *12*, 1918. https://doi.org/10.3390/ma12121918.

[2] Li, C.; McLinden, C.; Fioletov, V.; Krotkov, N.; Carn, S.; Joiner, J.; Dickerson, R.R. (2017). India is overtaking China as the world's largest emitter of anthropogenic sulfur dioxide. *Scientific Reports*, *7*, 14304. https://doi.org/10.1038/s41598-017-14639-8.

[3] Klotz, K.; Weistenhöfer, W.; Neff, F.; Hartwig, A.; van Thriel, C.; Drexler, H. (2017). The health effects of aluminum exposure. *Deutsches Ärzteblatt International*, *114*, 653. https://doi.org/10.3238/arztebl.2017.0653.

[4] Uddin, S.M.H.; Mostafa, M.G.; Haque, A.B.M.H. (2011). Evaluation of groundwater quality and its suitability for drinking purpose in Rajshahi City, Bangladesh. *Water Science and Technology: Water Supply*, *11*, 545–559. https://doi.org/10.2166/ws.2011.079.

[5] Hasan, S.; Ali, M.A. (2010). Occurrence of manganese in groundwater of Bangladesh and its implications on safe water supply. *Journal of Civil Engineering*, *32*, 121–128.

[6] Islam, M.S.; Mostafa, M.G. (2024). Impacts of Climate Change on Global Freshwater Quality and Availability: A Comprehensive Review. *Journal of Water and Environment Technology*, *22*, 1–26. https://doi.org/10.2965/jwet.23-036.

[7] Islam, M.Z.; Mostafa, M.G. (2024a). Iron, manganese, and lead contamination in groundwater of Bangladesh: A review. *Water Practice & Technology*, *19*, 745–760. https://doi.org/10.2166/wpt.2024.030.

[8] Mostafa, M.G.; Uddin, S.H.; Haque, A.B.M.H. (2017). Assessment of hydro-geochemistry and groundwater quality of Rajshahi City in Bangladesh. *Applied Water Science*, *7*, 4663–4671. https://doi.org/10.1007/s13201-017-0629-y.

[9] Islam, M.S.; Mostafa, M.G. (2021). Groundwater quality and risk assessment of heavy metal pollution in the middle-west part of Bangladesh. *Journal of Environmental Protection*, *3*, 1–5. https://doi.org/10.47363/JEESR/2021(3)143.

[10] Saha, N.; Zaman, M.R. (2011). Concentration of selected toxic metals in groundwater and some cereals grown in Shibganj area of Chapai Nawabganj, Rajshahi, Bangladesh. *Current Science*, 427–431.

[11] Islam, M.Z.; Mostafa, M.G. (2024). Suitability assessment of groundwater quality for drinking purposes. *Journal of Environmental Science and Sustainable Development*, *7*, 7. https://doi.org/10.7454/jessd.v7i1.1262.

[12] Islam, M.Z.; Mostafa, M.G. (2024). Seasonal variation of Fe, Mn, and Pb in groundwater of Northwestern Bangladesh. *Journal of Chemistry and Environment*, *3*, 77–97. https://doi.org/10.56946/jce.v3i1.296.

[13] Islam, M.R.; Mostafa, M.G. (2020). Characterization of textile dyeing effluent and its treatment using polyaluminum chloride. *Applied Water Science*, *10*, 119. https://doi.org/10.1007/s13201-020-01204-4.

[14] Mahdavi, S.; Jalali, M.; Afkhami, A. (2013). Heavy metals removal from aqueous solutions using $TiO_2$, MgO, and $Al_2O_3$ nanoparticles. *Chemical Engineering Communications*, *200*, 448–470. https://doi.org/10.1080/00986445.2012.686939.

[15] Mostafa, M.G.; Jan Hoinkis. (2012). Nanoparticles adsorbent for arsenic removal from drinking water: A review. *International Journal of Environmental Science, Management and Engineering Research*, *1*, 20–31.

[16] Mahdavi, S.; Jalali, M.; Afkhami, A. (2015). Heavy metals removal from aqueous solutions by $Al_2O_3$ nanoparticles modified with natural and chemical modifiers. *Clean Technologies and Environmental Policy*, *17*, 85–102. https://doi.org/10.1007/s10098-014-0764-1.

[17] Mostafa, M.G.; Chen, Y.-H.; Jean, J.-S.; Liu, C.-C.; Teng, H. (2010). Adsorption and desorption properties of arsenate onto nano-sized iron oxide-coated quartz. *Water Science and Technology*, *62*, 378–386. https://doi.org/10.2166/wst.2010.288.

[18] Nduni, M.N.; Osano, A.M.; Chaka, B. (2021). Synthesis and characterization of aluminium oxide nanoparticles from waste aluminium foil and potential application in aluminium-ion cell. *Cleaner Engineering and Technology*, *3*, 100108. https://doi.org/10.1016/j.clet.2021.100108.

[19] Sangor, F.I.; Al-Ghouti, M.A. (2023). Waste-to-value: Synthesis of nano-aluminum oxide (nano-$\gamma$-$Al_2O_3$) from waste aluminum foils for efficient adsorption of methylene blue dye. *Case Studies in Chemical and Environmental Engineering*, *8*, 100394. https://doi.org/10.1016/j.cscee.2023.100394.

[20] Mostafa, M.G.; Chen, Y.H.; Jean, J.S.; Liu, C.C.; Lee, Y.C. (2011). Kinetics and mechanism of arsenate removal by nanosized iron oxide-coated perlite. *Journal of Hazardous Materials*, *187*, 89–95. https://doi.org/10.1016/j.jhazmat.2010.12.117.

[21] Afkhami, A.; Saber-Tehrani, M.; Bagheri, H. (2010). Simultaneous removal of heavy-metal ions in wastewater samples using nano-alumina modified with 2, 4-dinitrophenylhydrazine. *Journal of Hazardous Materials*, *181*, 836–844. https://doi.org/10.1016/j.jhazmat.2010.05.089.

[22] Iijima, S.; Yumura, T.; Liu, Z. (2016). One-dimensional nanowires of pseudoboehmite (aluminum oxyhydroxide $\gamma$-AlOOH). *Proceedings of the National Academy of Sciences*, *113*, 11759–11764. https://doi.org/10.1073/pnas.1614059113.

[23] Feret, F.R.; Roy, D.; Boulanger, C. (2000). Determination of alpha and beta alumina in ceramic alumina by X-ray diffraction. *Spectrochimica Acta Part B: Atomic Spectroscopy*, *55*, 1051–1061. https://doi.org/10.1016/S0584-8547(00)00225-1.

[24] Paglia, G.; Buckley, C.E.; Udovic, T.J.; Rohl, A.L.; Jones, F.; Maitland, C.F.; Connolly, J. (2004). Boehmite-derived $\gamma$-alumina system. 2. Consideration of hydrogen and surface effects. *Chemistry of Materials*, *16*, 1914–1923. https://doi.org/10.1021/cm035193e.

[25] Dehghanian, H.; Farrash, S.M.H.; Jafari, M. (2024). Effect of moisture absorption on the flexural strength of phenolic matrix composites reinforced with glass fibers and aluminum oxide nanoparticles. *Polymer Composites*, *45*, 388–397. https://doi.org/10.1002/pc.27784.

[26] Atrak, K.; Ramazani, A.; Taghavi Fardood, S. (2018). Green synthesis of amorphous and gamma aluminum oxide nanoparticles by tragacanth gel and comparison of their photocatalytic activity for the degradation of organic dyes. *Journal of Materials Science: Materials in Electronics*, *29*, 8347–8353. https://doi.org/10.1007/s10854-018-8845-2.

[27] Ates, M.; Demir, V.; Arslan, Z.; Daniels, J.; Farah, I.O.; Bogatu, C. (2015). Evaluation of alpha and gamma aluminum oxide nanoparticle accumulation, toxicity, and depuration in *Artemia salina* larvae. *Environmental Toxicology*, *30*, 109–118. https://doi.org/10.1002/tox.21917.

[28] Trettenhahn, G.L.J.; Nauer, G.E.; Neckel, A. (1993). Vibrational spectroscopy on the PbO-$PbSO_4$ system and some related compounds: part 1. Fundamentals, infrared and Raman spectroscopy. *Vibrational Spectroscopy*, *5*, 85–100. https://doi.org/10.1016/0924-2031(93)87058-2.

[29] Mast, J.; Verleysen, E.; Hodoroaba, V.D.; Kaegi, R. (2020). Characterization of nanomaterials by transmission electron microscopy: Measurement procedures. In Characterization of Nanoparticles; Hodoroaba, V.D., Unger, W.E.E., Shard, A.G., Eds.; Elsevier, pp. 29–48. https://doi.org/10.1016/B978-0-12-814182-3.00004-3.

[30] Banerjee, S.; Dubey, S.; Gautam, R.K.; Chattopadhyaya, M.C.; Sharma, Y.C. (2019). Adsorption characteristics of alumina nanoparticles for the removal of hazardous dye, Orange G from aqueous solutions. *Arabian Journal of Chemistry*, *12*, 5339–5354. https://doi.org/10.1016/j.arabjc.2016.12.016.

[31] Rozita, Y.; Brydson, R.; Scott, A.J. (2010, July). An investigation of commercial gamma-$Al_2O_3$ nanoparticles. *Journal of Physics: Conference Series*, *241*, 012096. https://doi.org/10.1088/1742-6596/241/1/012096.

[32] Tabesh, S.; Davar, F.; Loghman-Estarki, M.R. (2018). Preparation of γ-$Al_2O_3$ nanoparticles using modified sol-gel method and its use for the adsorption of lead and cadmium ions. *Journal of Alloys and Compounds*, *730*, 441-449. https://doi.org/10.1016/j.jallcom.2017.09.246.

[33] Borandegi, M.; Nezamzadeh-Ejhieh, A. (2015). Enhanced removal efficiency of clinoptilolite nanoparticles toward Co(II) from aqueous solution by modification with glutamic acid. *Colloids and Surfaces A: Physicochemical and Engineering Aspects*, *479*, 35–45. https://doi.org/10.1016/j.colsurfa.2015.03.040.

[34] Bhat, A.; Megeri, G.B.; Thomas, C.; Bhargava, H.; Jeevitha, C.; Chandrashekar, S.; Madhu, G.M. (2015). Adsorption and optimization studies of lead from aqueous solution using γ-Alumina. *Journal of Environmental Chemical Engineering*, *3*(1), 30–39. https://doi.org/10.1016/j.jece.2014.11.014.

[35] Suresh Jeyakumar, R.P.; Chandrasekaran, V. (2014). Adsorption of lead (II) ions by activated carbons prepared from marine green algae: equilibrium and kinetics studies. *International Journal of Industrial Chemistry*, *5*, 1-10. https://doi.org/10.1186/s40090-014-0002-7.

[36] Mahmoodi, N.M.; Mokhtari-Shourijeh, Z. (2016). Modified poly(vinyl alcohol)-triethylenetetramine nanofiber by glutaraldehyde: preparation and dye removal ability from wastewater. *Desalination and Water Treatment*, *57*(42), 20076–20083. https://doi.org/10.1080/19443994.2015.1109562.

[37] Mohamed, H.S.; Soliman, N.K.; Abdelrheem, D.A.; Ramadan, A.A.; Elghandour, A.H.; Ahmed, S.A. (2019). Adsorption of $Cd^{2+}$ and $Cr^{3+}$ ions from aqueous solutions by using residue of Padina gymnospora waste as promising low-cost adsorbent. *Heliyon*, *5*(3). https://doi.org/10.1016/j.heliyon.2019.e01287.

[38] Gupta, V.K.; Ali, I. (2004). Removal of lead and chromium from wastewater using bagasse fly ash—a sugar industry waste. *Journal of Colloid and Interface Science*, *271*(2), 321–328. https://doi.org/10.1016/j.jcis.2003.11.007.

[39] Mazloomi, F.; Jalali, M. (2016). Ammonium removal from aqueous solutions by natural Iranian zeolite in the presence of organic acids, cations and anions. *Journal of Environmental Chemical Engineering*, *4*(1), 240-249. https://doi.org/10.1016/j.jece.2015.11.001.

[40] Ajala, E.O.; Aliyu, M.O.; Ajala, M.A.; Mamba, G.; Ndana, A.M.; Olatunde, T.S. (2024). Adsorption of lead and chromium ions from electroplating wastewater using plantain stalk modified by amorphous alumina developed from waste cans. *Scientific Reports*, *14*(1), 6055. https://doi.org/10.1038/s41598-024-56183-2.

[41] Mohamed, H.S.; Soliman, N.K.; Abdelrheem, D.A.; Ramadan, A.A.; Elghandour, A.H.; Ahmed, S.A. (2019). Adsorption of $Cd^{2+}$ and $Cr^{3+}$ ions from aqueous solutions by using residue of *Padina*

*gymnospora* waste as promising low-cost adsorbent. *Heliyon*, *5*(3). https://doi.org/10.1016/j.heliyon.2019.e01287.

[42] Naiya, T.K.; Bhattacharya, A.K.; Das, S.K. (2008). Removal of Cd (II) from aqueous solutions using clarified sludge. *Journal of Colloid and Interface Science*, *325*(1), 48–56. https://doi.org/10.1016/j.jcis.2008.06.003.

[43] Taiwo, A.F.; Chinyere, N.J. (2016). Sorption characteristics for multiple adsorption of heavy metal ions using activated carbon from Nigerian bamboo. *Journal of Materials Science and Chemical Engineering*, *4*(4), 39–48. https://doi.org/10.4236/msce.2016.44005.

[44] Wang, S.G.; Gong, W.X.; Liu, X.W.; Yao, Y.W.; Gao, B.Y.; Yue, Q.Y. (2007). Removal of lead (II) from aqueous solution by adsorption onto manganese oxide-coated carbon nanotubes. *Separation and Purification Technology*, *58*(1), 17–23. https://doi.org/10.1016/j.seppur.2007.07.006.

[45] Hohl, H.; Stumm, W. (1976). Interaction of $Pb^{2+}$ with hydrous γ-$Al_2O_3$. *Journal of Colloid and Interface Science*, *55*(2), 281–288. https://doi.org/10.1016/0021-9797(76)90035-7.

[46] Kovačević, D., Pohlmeier, A., Özbaş, G., Narres, H. D., & Kallay, M. J. N. (2000). The adsorption of lead species on goethite. *Colloids and Surfaces A: Physicochemical and Engineering Aspects*, *166*(1–3), 225–233. https://doi.org/10.1016/S0927-7757(99)00449-5.